

We are IntechOpen, the world's leading publisher of Open Access books Built by scientists, for scientists

6,900

Open access books available

186,000

International authors and editors

200M

Downloads

Our authors are among the

154

Countries delivered to

TOP 1%

most cited scientists

12.2%

Contributors from top 500 universities



WEB OF SCIENCE™

Selection of our books indexed in the Book Citation Index
in Web of Science™ Core Collection (BKCI)

Interested in publishing with us?
Contact book.department@intechopen.com

Numbers displayed above are based on latest data collected.
For more information visit www.intechopen.com



Thermodynamics of Enthalpy Relaxation and Hole Formation of Polymer Glasses

Nobuyuki Tanaka
Gunma University, Tsutsumicho, Kiryu,
Japan

1. Introduction

The enthalpy relaxation of the glassy materials has been investigated rheologically for years with a view to approaching the ideal glass^{1 - 5}). The imaginary liquid at Kauzmann temperature^{2, 3}), T_K , at which the extrapolation line of enthalpy or entropy as a function of temperature for the liquid intersected the enthalpy or entropy line of the crystal, had been considered once to be the ideal glass. However because at T_K the enthalpy or entropy for the liquid was same as that of crystal, the liquid like this was hard to take thermodynamically, bringing the entropy crisis. Fig. 1 depicts the change of the enthalpy difference, ΔH , between the liquid and the crystal upon cooling for a polymer. For stable liquids, ΔH should be almost constant from near T_g upon cooling as described below. Therefore, the liquid line can never intersect that of the crystal. The transition from liquid to crystal or vice versa means the emission or absorption of the latent heat accompanying the enthalpy jump. Thus for polymers, T_K is merely a temperature parameter.

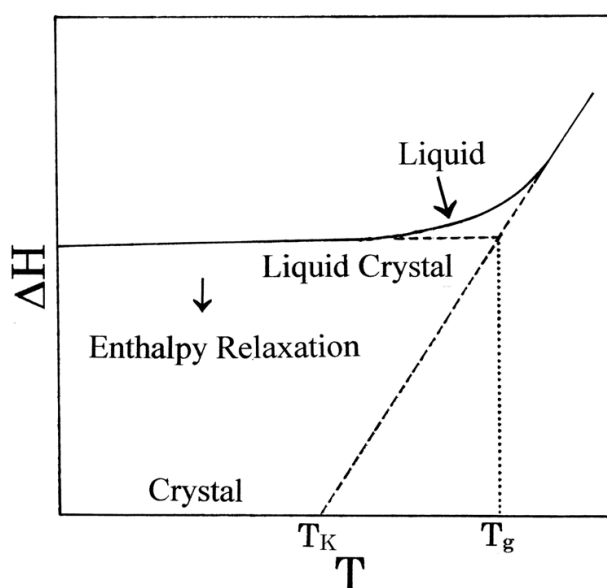


Fig. 1. The change of ΔH for a polymer liquid or liquid crystal (solid line) upon cooling. The small arrow mark shows the direction of enthalpy relaxation. The base line is that of crystal. The dashed lines are extrapolated to T_g and T_K , and the dot line is complementary.

For the glass transition of polymeric or other matter glasses, whether it is the phase transition or not is nowadays yet controversial^{6 - 11}). However for polymers, the criterion of the glass transition temperature, T_g , presented by us is decisive, supporting the first order hole phase transition^{12 - 14}) and the broad heat capacity jump at the glass transition without the enthalpy relaxation has been understood successfully¹⁵). The cooled polymers unidentified by the criterion should belong to the liquid on the way of enthalpy relaxation even if they were glassy. When without the enthalpy relaxation at temperatures below T_g , the super-cooled liquid could be stable thermodynamically. Glassy pitch⁴) might be the stable liquid, which is flowing still at a drop per 9 years from 1927. Recently, for poly(ethylene terephthalate) (PET)¹⁶), polystyrene (PS), isotactic polypropylene (iPP), polyethylene (PE) and nylon-6 (N6), it was predicted that during the enthalpy relaxation at temperatures below T_g , the "ordered part / hole" pairs should generate and consequently, bringing a reduction in the relaxation time to the goal of the ideal glass, e.g., the quasi-crystals lacked periodicity but with symmetry¹⁷), the alternative and stable glass parts should be formed between their pairs. At T_g , the unfreezing of glass parts is caused by the first order hole phase transition. Then the holes should play the free volume jump as an affair of dynamic equilibrium in the disappearance and generation of "ordered part / hole" pairs. The free volume jump at the glass transition, accompanying the enthalpy and entropy jumps, is the characteristic of the first order hole phase transition. In this chapter, introducing the constant volume heat capacity of photons to the holes^{16, 18, 19}), the generation of "ordered part / hole" pairs during the enthalpy relaxation at temperatures below T_g and the subsequent disappearance at the glass transition, accompanied by the jumps of free volume, enthalpy and entropy, were discussed for PET, PS, iPP, PE and N6 on the basis of thermodynamics. IPP, PE and N6 were investigated as the peculiar cases for the comparison with PET and PS, which are the glassy polymers with the almost same values of the constant, c_2 , of WLF equation²⁰), i.e., 55.3 K²¹) and 56.6 K²⁰), respectively. The holes taken in the helix structure of iPP should hold the interaction of partnership with the helical ordered parts. For PE, the glasses with $T_g = 135$ K and 237 K depending on the structure of the ordered parts¹⁵) were discussed. It seems likely that from near 130 K, the growth of open space in the PE glasses occurs²²). DSC (Differential Scanning Calorimetry) on PE films¹⁸) revealed that ~38 % of the crystal lamella was constituted by the inter-grain aggregates containing the glass with a secondary T_g . The generation of "crystal / anti-crystal hole" pairs from the secondary glass was discussed. For N6, the ordered parts were the stretched sequences of $-(CH_2)_5-$ between amido groups. The hole energy of "ordered part / hole" pairs was concerned with the frequency of absorption bands in the infrared spectrum.

2. Enthalpy relaxation and hole formation of PET, PS, iPP, PE and N6 glasses

2.1 Thermodynamics of glass transition

The glass transition temperature, T_g , of polymer glasses could be identified as that of the first order hole phase transition by satisfying the criterion consisted of Eqs. (1) and (2), in which f_x has been added under the operational definition concluding that the stable glasses could not be formed easily without the generation of "ordered part / hole" pairs during the enthalpy relaxation at temperatures below T_g ¹³):

$$f_x = f_{\text{flow}} (= h_{\text{flow}} - T_g S_{\text{flow}}) = 0 \quad (1)$$

$$s_{\text{flow}} = 0 (\because h_{\text{flow}} = 0) \quad (2)$$

where $f_x (= h_x - T_g s_x)$, h_x and s_x are the free energy, enthalpy and entropy per molar structural unit for ordered parts, f_{flow} , h_{flow} and s_{flow} are the free energy, enthalpy and entropy per molar structural unit for flow parts. The molar free energy of holes held photons at the temperature, T , is generally given by $f^h = -RT \ln(v_f/v_0)$ and then the molar entropy of holes, s^h , at a constant pressure, p , is derived:

$$s^h = -(\partial f^h / \partial T)_p = R \ln(v_f/v_0) + RT \{ \partial \ln(v_f/v_0) / \partial T \}_p \quad (3)$$

where v_f and v_0 are the molar free and core volumes of holes and R is the gas constant. When v_0 is almost constant, from $f^h = h^h - T s^h$ and Eq. (3), the molar enthalpy of holes, h^h , is derived:

$$h^h = RT^2 (\partial \ln v_f / \partial T)_p \quad (4)$$

When the ordered parts at T_g are in equilibrium with the holes; $f_x (= 0) = f^h$, from $f_x = 0$ and $h_x = h_g + \Delta h$ (see Eq. (13)), s_x at T_g is derived:

$$s_x (= h_x / T_g) = \Delta s_g + \Delta h / T_g \quad (5)$$

with $\Delta s_g = h_g / T_g$, defining the entropy of unfreezing for the glass parts at T_g , where h_g is the molar glass transition enthalpy, Δh is the heat per molar structural unit required still to melt ordered parts, relating to the jump of v_f (see Eq. (8)). Further from Eq. (2), the h_g and the molar glass transition entropy, s_g , are derived¹³⁾:

$$h_g = RT_g^2 (\partial \ln v_f / \partial T)_p \quad (6)$$

$$s_g (= s_g^{\text{conf}} + s_g^{\text{int}}) = R \ln(v_f/v_0) + RT_g (\partial \ln v_f / \partial T)_p \quad (7)$$

with $s_g^{\text{int}} = (3R/2) \ln(2\pi m k T_g / h^2) - (1/x)(R/N) \ln N! + R \ln q - R \ln v_0$

where s_g^{conf} and s_g^{int} are the conformational and cohesive entropies per molar structural unit for glass parts at T_g (see Eq. (16) for s_g^{conf}), m is the mass of a structural unit, k is Boltzmann constant, h is Planck constant, N is the number of chains, x is the degree of polymerization and q (≤ 1) is the packing factor. When $v_f = v_0$, from Eqs. (6) and (7), $h_g = 0$ and $s_g = 0$ are derived. On the other hand, from $f^h = 0 (= f_x)$ at T_g , h^h is given as:

$$h^h = RT_g^2 (\partial \ln v_f / \partial T)_p + RT_g \ln(v_f/v_0) \quad (8)$$

In the case of $RT_g \ln(v_f/v_0) = \Delta h$, the relation of $h_x = h^h$ is derived from Eq. (8), because of $RT_g^2 (\partial \ln v_f / \partial T)_p = h_g$. However, when the length distribution by lengthening of ordered parts occurred during the enthalpy relaxation at temperatures below T_g , as longer the length of ordered parts, the melting temperature, T_x , for ordered parts should be elevated from T_g to the higher temperature²³⁾ (see Eq. (29)). Therefore the shortage of $\Delta h (= RT_g \ln(v_f/v_0))$ corresponding to the latent heat of disappearance for the holes at T_g is made up by the supply of the heat required to melt all ordered parts:

$$\Delta h = \int_{T_g}^{T_x} \Delta C_p dT \quad (9)$$

where T_ℓ is the end temperature of melting for ordered parts, ΔC_p is the difference between the observed isobaric heat capacity, C_p^ℓ , for the equilibrium liquid and C_p^g for the hypothesized super-heated glass at the glass transition from T_g to T_ℓ . In the equilibrium liquid, the isobaric heat capacities of ordered parts and flow parts, C_p^x and C_p^{flow} , are equal to C_p^ℓ , respectively¹³:

$$C_p^\ell = C_p^x = C_p^{\text{flow}} \quad (10)$$

In the flow parts, the tube-like space exists between a chain and the neighboring chains, behaving as if it is the counterpart of a chain²⁴). Therefore when the hole energy at $T (> T_g)$ is given by $\varepsilon (= 3C_{v,\text{ph}}T)$, C_p^{flow} is represented as¹⁶):

$$C_p^{\text{flow}} = 3C_{v,\text{ph}}(1 + T \text{dln}J/\text{dT}) \quad (11)$$

where $C_{v,\text{ph}} (= 2.701R)^{16, 18, 19}$ is the constant volume heat capacity for photons, J is the number of holes lost by T and 3 is the degree of freedom for photons.

Fig. 2 shows the schematic curves of the molar entropy, s , and the v_f around T_g upon cooling and heating for polymers. Upon cooling in Fig. 2 (upper), the dashed line is the s curve for the liquid glass frozen partially from the super-cooled liquid and the solid line upon heating

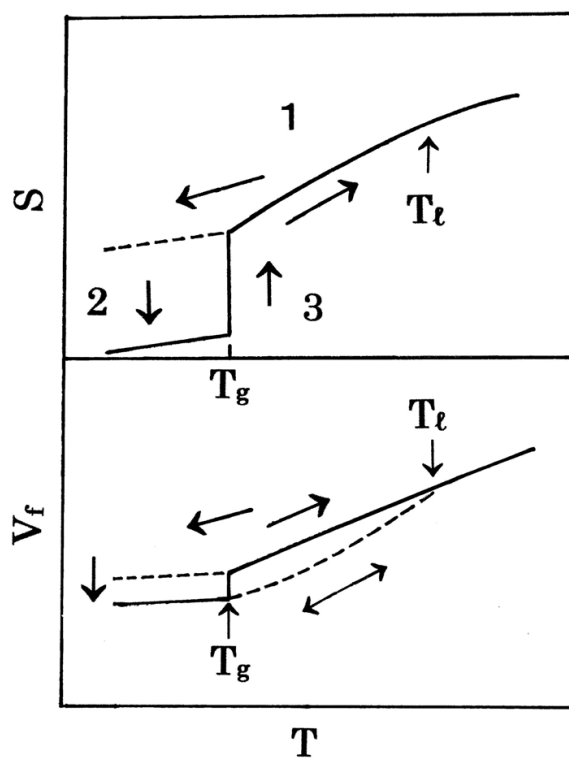


Fig. 2. The schematic curves of the entropy, s , and the free volume, v_f , around T_g for polymers. Upper; **1**: the change of s for the liquid glass frozen partially from the super-cooled liquid, shown by the dashed line, **2**: the entropy relaxation and **3**: the change of s with a jump at T_g upon heating. Lower; The dashed line upon cooling is the v_f curve for the same liquid glass, the solid line upon heating after relaxation shows the v_f curve with a jump at T_g and the dashed line shows a reversible jump of v_f between T_g and T_ℓ .

after relaxation shows the subsequent s curve with a jump at T_g . Upon cooling in Fig. 2 (lower), the dashed line is the v_f curve for the same liquid glass. Upon heating after relaxation, the solid line shows the v_f curve with a jump at T_g and the dashed line shows a reversible jump of v_f between T_g and T_t .

2.2 “Ordered part / hole” pairs

Next whether h_x agrees to h^h at T_g or not is investigated for PET, iPP, PS, PE and N6 glasses. The agreement provides one of evidences for the generation of “ordered part / hole” pairs during the enthalpy relaxation at $T (< T_g)$. h^h at T_g is given by¹⁶⁾:

$$h^h = 3C_{v,ph}T_g \quad (12)$$

where $C_{v,ph} = 2.701R$. For PET with $T_g = 342$ K, $h^h = 23.0$ kJ/mol was derived. While h_x at T_g is given by^{13, 25)}:

$$h_x = h_g + \Delta h \quad (13)$$

In Eq. (13), h_g is given approximately by three expressions^{13, 25)}; (1) RT_g^2/c_2 (c_2 is the constant of WLF equation²⁰⁾), (2) the molar enthalpy difference between the super-cooled liquid and the crystal at T_g , $H_g^a - H_g^c$, and (3) the sum of the conformational and cohesive enthalpies per molar structural unit at T_g , $h_g^{conf} + h_g^{int}$. Δh is given by either Eq. (14) or (15)^{25, 26)}:

$$\Delta h = \Delta H - Q \quad (14)$$

with $\Delta H = H_m^a - H_c^a$, where H_m^a is the enthalpy per molar structural unit for the liquid at the equilibrium melting temperature, T_m^∞ , H_c^a is the enthalpy per molar structural unit for the super-cooled liquid at the onset temperature, T_c , of a DSC crystallization peak upon cooling and Q is the heat per molar structural unit corresponding to the total area of the DSC endothermic peak upon heating. Or, rewriting Eq. (13),

$$\Delta h = (h_x^{conf} - h_g^{conf}) + \Delta h^{int} \quad (15)$$

where h_x^{conf} is the conformational enthalpy per molar structural unit for ordered parts, Δh^{int} is the molar cohesive enthalpy difference between the ordered parts and the glass parts. Thus when $h_x^{conf} = h_g^{conf}$ at T_g , $\Delta h = \Delta h^{int} = (RT_g \ln Z_t)/x$ (see Table 3 for N6) and when $h_x^{conf} \neq h_g^{conf} = 0$ at T_g , the another Δh is derived^{26, 27)}.

$$\Delta h = T_g \{s_g^{conf} - (R \ln Z_0)/x\} \quad (16)$$

with $s_g^{conf} = (R \ln Z + RT_g d \ln Z / dT) / x$

where Z is the conformational partition function for a chain, $Z_0 (= Z/Z_t)$ and Z_t are the component conformational partition function for a chain regardless of temperature and as a function of temperature, respectively. The differential of Eq. (15) by temperature represents the heat capacity jump at the glass transition¹⁵⁾.

Table 1 shows the values of T_g , Δs_g , h_g , Δh , h_x , h^h and h^h/h_x for PET, iPP and PS. PET showed the good agreement between h_x , i.e., 22.3 ~ 24.1 kJ/mol, and h^h , i.e., 23.0 kJ/mol. The values of them also agreed with the heat of fusion, $h_u = 23.0$ kJ/mol, for the smectic crystals of mesophase with the conformational disorder between the phenylene groups but along

Polymer	T_g K	Δs_g J/(K mol)	h_g kJ/mol	Δh kJ/mol	h_x kJ/mol	h^h kJ/mol	h^h/h_x
PET	342	47.1	16.1* ¹	6.5* ⁴	22.6	23.0	1.0
		51.5	17.6* ²	6.2* ⁵	23.8		1.0
		51.2	17.5* ³	6.2* ⁵	23.7		1.0
iPP	270	23.0	6.2* ¹	1.1* ⁴	7.3	18.2	2.5 (1.0* ⁷)
		23.7	6.4* ³	1.0* ⁵	7.4		2.5 (1.0* ⁷)
PS	359	52.6	18.9* ²	5.3	24.2* ⁶	24.2	1.0
		56.5	20.3* ³	3.9	24.2* ⁶		1.0

*¹: $H_g^a - H_g^c$, *²: RT_g^2/c_2 , *³: $h_g^{conf} + h_g^{int}$, *⁴: Eq. (14), *⁵: Eq. (16), *⁶: $h_x = h^h$ and *⁷: $(h^h/2.5)/h_x$. The data of iPP used to calculate Δh in Eq. (14) are as follows: $T_c = 403.6$ K, $T_m^\infty = 449$ K for the α form crystal²⁸), $\Delta H (=H_m^a - H_c^a) = 4.89$ kJ/mol²⁹) and $Q = 3.76$ kJ/mol for the sample annealed at 461.0 K for 1 hour.

Table 1. The values of T_g , Δs_g , h_g , Δh , h_x , h^h and h^h/h_x for PET, iPP and PS.

a chain axis^{25, 30}). For the smectic-c crystals with stretched sequences, h_u is 28.5 kJ/mol. Further, DSC revealed²⁵) that for the crystalline films of smectic-c crystals, the ordered parts in the amorphous regions were like smectic crystals and for the crystalline films of smectic crystals, the ordered parts were like the smectic-c crystals. Fig. 3 shows the sequence models of smectic crystal (A) and smectic-c crystal (B), together with the four conformations (a, b, c and d) that an isolated chain can take preferentially below 10 K. An arrow mark shows the direction of ordering or crystallization for a, b, c and d. From these results, the ordered parts are like the smectic crystal and the hole of a pair should have the free volume coming from the difference of conformation between A and a, b, c or d in Fig. 3. For iPP, h^h was 2.5 times as much as h_x . This result suggested that the hole of a pair was the inside space of a 3/1 helical ordered part composed of 3 structural units, holding 3 photons, but each photon was concerned in the potential energy of 2.5 structural units in a helical sequence, and that, $(h^h/2.5)/h_x = 1$. This was comparable to $h^h/h_x = 1$ for PET. The value of

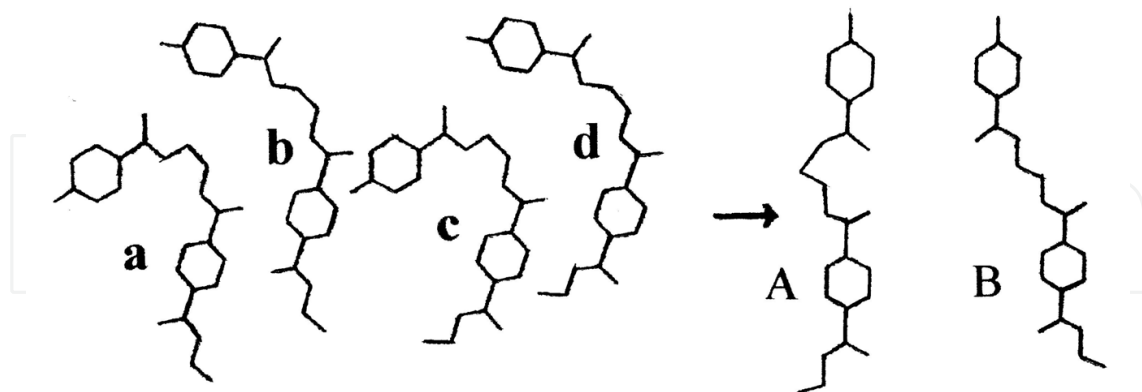


Fig. 3. Right: The sequence models of the smectic crystal of mesophase with a conformational disorder (A) and the smectic-c crystal with a stretched conformation (B) for PET³⁰). Left: Four conformations taken preferentially below 10 K for an isolated chain; a: TTTTG'T, b: TTTTGT, c: TCTTG'T and d: TCTTGT, by Flory's theory³¹). T, G and G' are the trans, gauche and gauche' isomers, respectively. T and C are the trans and cis isomers of phenylene groups (lower groups). An arrow mark shows the direction of ordering or crystallization.

h_x was almost equal to h_u ($= 7.6$ kJ/mol for α form). Fig. 4 shows the photon sites in the helix structure and the helical conformation of an isolated sequence with an inversion defect isomer TT , taking preferentially at temperatures below 70 K²⁶).

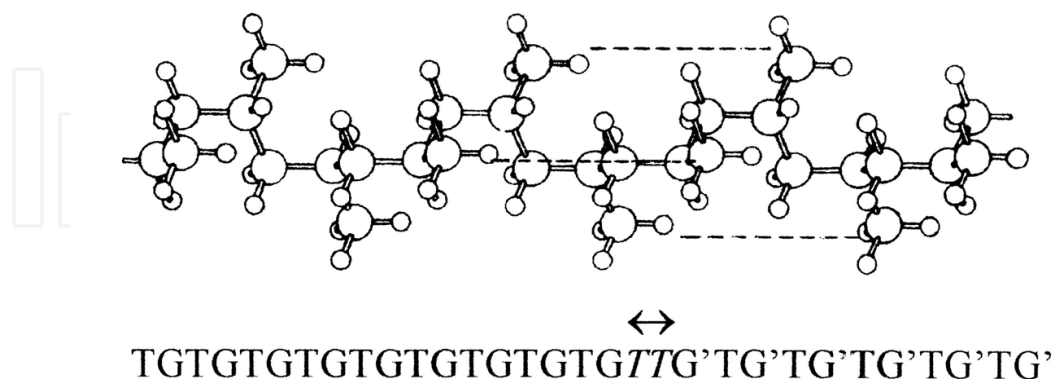


Fig. 4. Upper: The photon sites (the dashed line parts) in the helix structure with TGTG or TG'TG' conformation at temperatures below T_g for iPP. Large circle: C and small circle: H. Lower: The helical conformation of an isolated sequence with an inversion defect isomer TT , taking preferentially at temperatures below 70 K. The allow mark shows the shift of TT on a helical sequence.

For PS, supposing $h_x = h^h$, Δh was evaluated. From the value of Δh to be near that of PET, the v_f jump at T_g should be due to the release between phenyl groups. The T_g of PE¹⁵), producing the entropy of unfreezing for the glass parts; $\Delta s_g = h_g/T_g$ (see Eq. (5)), was almost dependent on h_g^{int} . When a value of h_g^{int} was that of the glass with $T_g = 237$ K, $h_g^{int}/2$ gave $T_g = 135$ K. Table 2 shows the values of T_g , Δs_g , h_g , Δh , h_x , h^h and h^h/h_x for PE glasses with $T_g = 135$ K ($h_g^{int} = 2.8/2$ kJ/mol) and 237 K ($h_g^{int} = 2.8$ kJ/mol). The above relation in T_g and h_g^{int} for the glass parts was linked to the ordered parts. For both glasses, h^h was about 5 times as much as h_g . Thus from Eq. (13), the common relations of $h_x = h^h/4$ and $\Delta h = h^h/4 - h_g$ were predicted for the ordered parts in both glasses and shown in Table 2. Fig. 5 depicts the sequence models of ordered parts (A and B) and the schematic transition from the glassy state (C: left) to that of the "ordered part / hole" pair (C: right).

For the glass with $T_g = 135$ K, the coarse 4/1 helical ordered parts with GG or G'G' conformation in Fig. 5A and as the hole of a pair, the inside space holding four photons per a helical segmental unit, $-(CH_2)_4-$, were predicted. Further the length distribution of helical ordered parts in the glass and as the end temperature of melting for the ordered parts, ~ 237 K were predicted. In this case, the same value of Δh for both glasses enabled the scheme as depicted in Fig. 6. For the glass with $T_g = 237$ K, the ordered part of fringe-type formed by

Polymer	T_g K	Δs_g J/(K mol)	h_g kJ/mol	Δh kJ/mol	h_x kJ/mol	h^h kJ/mol	h^h/h_x
PE	135	13.8	1.8* ¹	0.5	2.3* ²	9.1	4 (1* ³)
	237	14.8	3.5* ¹	0.5	4.0* ²	16.0	4 (1* ³)

*1: $h_g^{conf} + h_g^{int}$, *2: $h_x = h^h/4$ and *3: $(h^h/4)/h_x$.

Table 2. The values of T_g , Δs_g , h_g , Δh , h_x , h^h and h^h/h_x for PE.

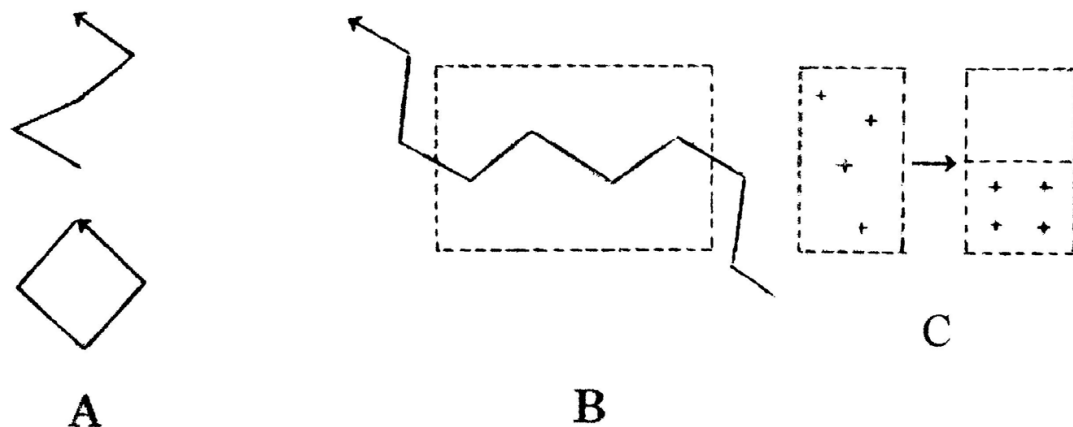


Fig. 5. The sequence models of ordered parts; A: the 4/1 helix structure and B: the stretched structure in the region surrounded by the dashed line. C (left): the glassy state and C (right): the state of a "ordered part / hole" pair. The plus mark (+) shows the cross section of a stretched segmental unit, $-(\text{CH}_2)_4-$. An arrow mark shows the direction of ordering.

bundling TTT parts of four sequences at least, and that, the smallest crystal of PE and the neighboring hole were predicted (see Fig. 5B and C: right), since the value of h_x was almost equal to $h_u = 4.1$ kJ/mol. Fig. 6 shows the bar graph of h_g at $T_g = 135$ K and 237 K, together with $\Delta h (= 0.5$ kJ/mol) at 237 K, for PE. The difference in two complementary lines suggests the supply schedule of heat over the temperature range from 135 K to ~ 237 K in order to make up the shortage of Δh required to melt all ordered parts in the glass with $T_g = 135$ K. For the glass with $T_g = 237$ K, the glass transition only at T_g is shown. The enthalpy relaxation, accompanied by the generation of stretched segments, at temperatures over 135 K to ~ 237 K

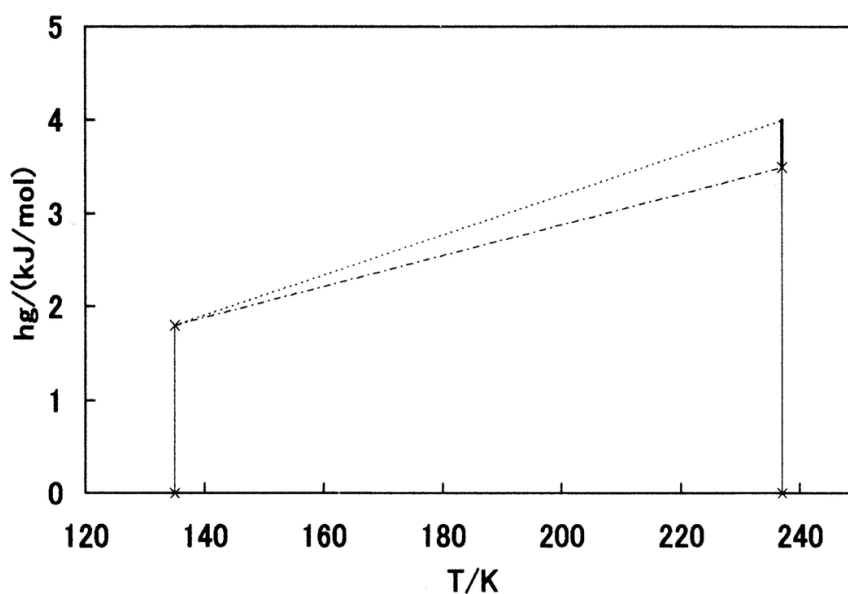


Fig. 6. The bar graph of h_g at $T_g = 135$ K and 237 K (the vertical thin lines between the cross marks) and $\Delta h (= 0.5$ kJ/mol) at 237 K (the thick line part) for PE. The dot and dot-dashed lines are drawn complementarily.

should vitrify or order the melted helical ordered parts and confine the larger helical ordered parts, which were not yet melted even over $T_g = 135$ K, in the glass. The liquid on the way of enthalpy relaxation like this should reach step by step to the glass with $T_g = 237$ K ($h_g^{\text{int}} = 2.8$ kJ/mol) at temperatures below T_g . Table 3 shows the values of T_g , Δs_g , h_g , Δh , h_x , h_u and h^h for N6. For N6, $h_g^{\text{conf}} = h_x^{\text{conf}}$ in Eq. (15), i.e., $\Delta h = (RT_g \ln Z_t)/x$ was predicted, because of the strong interaction between amido groups. h^h was 4.7 times as much as h_x in the parenthesis. Accordingly a photon was concerned in the potential energy of a stretched segmental unit, $-(\text{CH}_2)_5^-$. Further $\Delta h = 2.5$ kJ/mol was 0.5 kJ per molar methylene unit, $-\text{CH}_2-$, which agreed with $\Delta h = 0.5$ kJ/mol for the PE glasses with $T_g = 135$ K and 237 K (see Table 2). In addition, the value of h^h was almost equal to h_u of the heat of fusion. This agreement suggested that the ordered parts were the stretched segmental units in the smallest crystals of N6. Fig. 7 shows the structural unit of N6 and the photon site in the structural unit.

Polymer	T_g K	Δs_g J/(K mol)	h_g kJ/mol	Δh^{*2} kJ/mol	h_x kJ/mol	h_u kJ/mol	h^h kJ/mol
N6 ²⁷⁾	313	120.1 (6.4)	37.6 ^{*1} (2.0)	2.5, 0.5 ^{*3}	40.1 (4.5)	21.3	21.1

*1: $h_g = h_g^{\text{conf}} + h_g^{\text{int}}$, *2: $\Delta h = (RT_g \ln Z_t)/x$ and *3: the value of Δh per molar methylene unit, $-\text{CH}_2-$. The values of Δs_g , h_g and h_x in the parentheses are those without the cohesive energy of amido group, 35.6 kJ/mol.

Table 3. The values of T_g , Δs_g , h_g , Δh , h_x , h_u and h^h for N6.

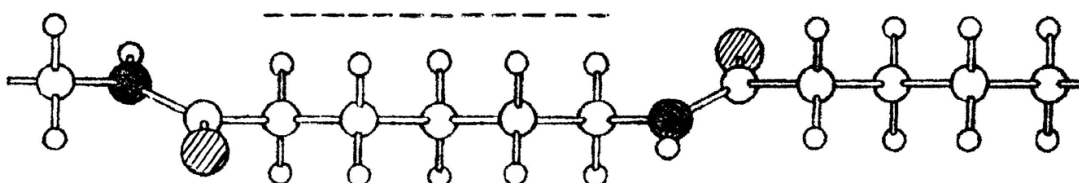


Fig. 7. The structure of N6 structural unit and the photon site (the dashed line part) in the unit. The filled circle: N, the shaded circle: O, the large circle: C, and the small circle: H.

3. Hole energy and a photon

A photon has the property as a boson or a wave. Therefore h^h is also represented as the vibrational energy of a wave with the quantum number $n = 1$ (meaning one photon) and the frequency per second (sec), ν :

$$h^h = N_A(3/2)h\nu \quad (17)$$

where N_A is Avogadro constant. Thus from Eqs. (12) and (17), the zero-point energy, $\epsilon_0 (= (1/2)h\nu)$, is derived:

$$\epsilon_0 = C_v^{\text{ph}}T_g/N_A \quad (18)$$

Table 4 shows the values of T_g , h^h , ν , λ and $1/\lambda$ for PE, iPP, PS and PET, where λ is the wavelength and $1/\lambda$ is the wavenumber. According to the infrared spectroscopy, for PE, $1/\lambda = 510 \text{ cm}^{-1}$ and 893 cm^{-1} might be concerned with 720 cm^{-1} and 731 cm^{-1} bands assigned to the rocking of $-\text{CH}_2-$ ³²). For iPP, $1/\lambda = 1022 \text{ cm}^{-1}$ almost agreed with 1045 cm^{-1} relating to the crystallinity³³). Also for PS, $1/\lambda = 1359 \text{ cm}^{-1}$ almost agreed with one of conformation sensitive bands³⁴), i.e., 1365 cm^{-1} band. For PET, $1/\lambda = 1292 \text{ cm}^{-1}$ was near 1339 cm^{-1} and 1371 cm^{-1} bands assigned to the wagging of $-\text{CH}_2-$ with trans and gauche conformations, respectively³⁵).

Polymer	T_g K	h^h kJ/mol	ν sec ⁻¹	λ μm	$1/\lambda$ cm^{-1}
PE	135	9.1	15.3×10^{12}	19.6	510
	237	16.0	26.9×10^{12}	11.2	893
iPP	270	18.2	30.6×10^{12}	9.78	1022
PS	359	24.2	40.6×10^{12}	7.36	1359
PET	342	23.0	38.6×10^{12}	7.74	1292

Table 4. The values of T_g , h^h , ν , λ and $1/\lambda$ for PE, iPP, PS and PET.

4. Conclusions and introduction to next section

For PET, PS, iPP, PE and N6 glasses, the generation of “ordered part / hole” pairs during the enthalpy relaxation at temperatures below T_g and the subsequent disappearance at the glass transition were discussed under the operational definition leading the criterion of T_g . Thus it was concluded that the unfreezing of the glass parts at T_g was caused by the first order hole phase transition, accompanied by the jumps of free volume, enthalpy and entropy. h^h was concerned with the frequency of the absorption bands in the infrared spectrum. In particular, $1/\lambda$ for iPP and PS coincided closely with the respective sensitive bands with physical meaning. In the next section, the generation of “crystal / anti-crystal hole” pairs from the secondary glass in PE crystal lamella was discussed on the DSC curves. The secondary glass was distinguished from the primary glass discussed in the above sections. The C_v^{ph} was also available in the discussion of the cavity radiation from the anti-crystal holes filled by photons. The anti-crystal holes were regarded as the lattice crystal made up of photons without the mass.

5. Crystallization of secondary glass in PE lamella

5.1 Thermal analysis

DSC is capable of quantitatively determining by way of standard and dynamical measurements³⁶) the common thermal phenomena in polymers, e.g., the melting, the crystallization and the glass transition. Such analyses are carried out on the basis of thermodynamics, mathematics and molecular dynamics simulation^{36, 37}). This section describes an attempt to understand the peculiar DSC curves of PE films containing orthorhombic crystals. DSC demonstrated two indications of the secondary glass in the crystal lamella. One of the underlying reasons was the much larger heat of melting as opposed to the heat of crystallization upon cooling and the other was the fact that the glass

transition enthalpy was larger than the molar enthalpy of the ordered parts in the amorphous regions; $\Delta h < 0$ in Eq. (14). At temperatures above its T_g , the generation and disappearance of the “crystal / anti-crystal hole” pairs from the secondary glass were predicted as the simultaneous phenomena in the crystallization and the melting. Hexagonal and monoclinic forms of PE crystals are also well known. However, the hexagonal crystals should not be related to the melting of the orthorhombic crystals since the DSC melting peak of the hexagonal crystals generally cannot be observed for the samples without restraints such as high pressure³⁸). Moreover, the DSC melting peak of monoclinic crystals disappears before the melting of the orthorhombic crystals^{39, 40}). Thus, when the monoclinic crystals are in the bulk state, the heat due to their melting should contribute to the activation heat required to release the secondary glass state in the orthorhombic crystal lamella.

5.2 Secondary glass

Fig. 8 depicts the DSC crystallization peak upon cooling and the two peaks divided from a DSC endothermic peak upon heating for the PE film annealed at 416.6 K (near $T_m^\infty = 415$ K) for 1 hour. The thin line in T_b^* and T_e^* is the curve before division. T_c ($= 391.5$ K) is the onset temperature of crystallization, T_b^* ($\approx T_c$) is the intersection between the base line and the extrapolation line from the line segment with the highest slope on the lower temperature side of the melting peak, and that, the onset temperature of the higher temperature side peak and T_e^* is the end temperature of the lower temperature side peak, and that, the origin of the extrapolation line, respectively. Q_m is the heat per molar structural unit corresponding to the endothermic peak area of crystal lamella that starts to melt at T_b^* and h_c ($= 0.89$ kJ/mol) is the heat of crystallization per molar structural unit corresponding to the area surrounded by the dashed line and the exothermic curve. ΔQ_m ($= Q_m - h_c$) corresponds to the area between T_b^* and T_e^* of the higher temperature side

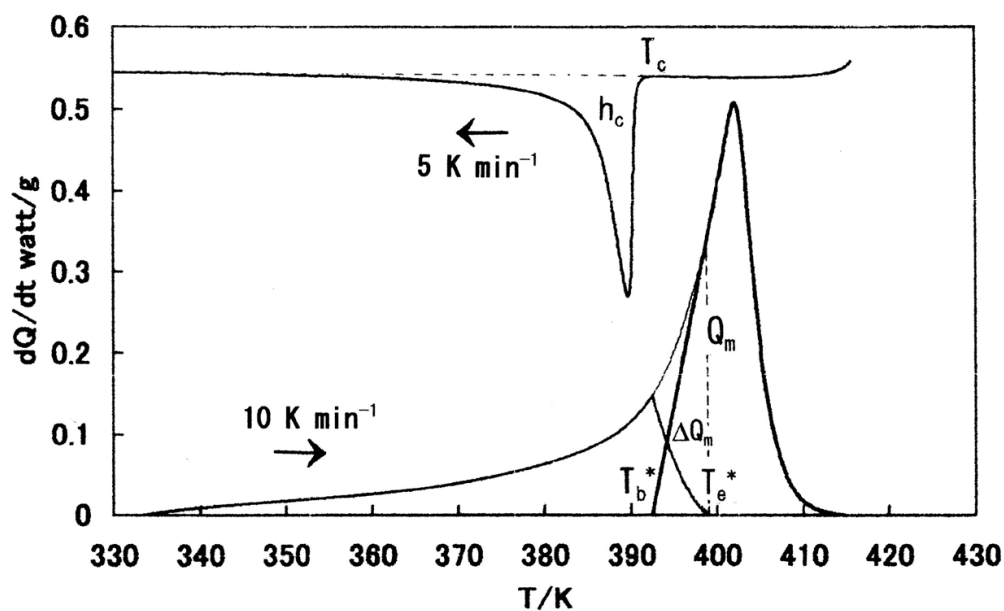


Fig. 8. The DSC crystallization peak upon cooling and the two peaks divided from a DSC endothermic peak upon heating for the PE film annealed at 416.6 K for 1 hour. dQ/dt is the heat flow rate. The cooling and heating rates are 5 K/min and 10 K/min, respectively.

peak, which is equal to the area surrounded by the thin line and the lower temperature side peak curve between T_b^* and T_c^* . The endothermic peak on the lower temperature side is due to the melting of small crystals around the crystal lamella⁴¹). The decrease of heat flow rate from T_b^* to T_c^* for the peak on the lower temperature side is believed to be due to the crystallization of secondary glass in the inter-grain aggregates belonging to the crystal lamella (see Fig. 9). This precedes the increase of heat flow rate due to the melting of newly crystallized parts from T_b^* to T_c^* in the peak on the higher temperature side. The equilibrium melting of the ordered parts in the amorphous regions does not show any peak. Its enthalpy, h_x , has been represented as Eq. (13), in which Δh given by Eq. (14) is usually positive; 6.5 kJ/mol and 11.5 kJ/mol for PET with two values of T_m^∞ (535 K and 549 K)²⁵, respectively. Also for iPP, Δh (= 1.1 kJ/mol) of Eq. (14) was positive, as shown in Table 1. Nevertheless, it was found to be negative for PE (see Table 5). In order to satisfy $\Delta h < 0$ ($h_g > h_x$), the glass with a secondary T_g , which formed near T_c upon cooling and disappeared near T_c after melting of the ordered parts in the amorphous regions upon heating, must exist in the crystal lamella. When the secondary T_g is approximated to T_c , h_g^* is given by:

$$h_g^* \approx H_c^a - H_c^c \quad (19)$$

where h_g^* is h_g at the secondary T_g , H_c^a and H_c^c are the enthalpy per molar structural unit for the super-cooled liquid and the crystal at T_c . h_x is given by $h_g^* + \Delta h$ ($\Delta h < 0$). Here, ΔH (= $H_m^a - H_c^a$) in Eq. (14) is regarded as the heat emitted when only one single crystal lamella without deformation is formed. According to the ATHAS databank²⁹), ΔH is 0.83 kJ/mol, which is close to the value of $h_c = 0.89$ kJ/mol as observed in Fig. 8. The difference in h_c and ΔH , 0.06 kJ/mol, might be the additive heat of emission due to the release of lamellar deformation. The spherulites observed in the films are substantially like disks⁴²). The twist deformation energy of ribbon-like lamella is believed to originate from the irregular growth of lamella. Fig. 9 shows a schematic structure of the crystal lamella after release of the twist deformation from the ribbon-like lamella. The dark parts between the rectangular parallelepiped blocks correspond to the inter-grain aggregates described above. The crystal lamellae for the samples used here are described in the section 5.5 of "Crystal length distribution function".

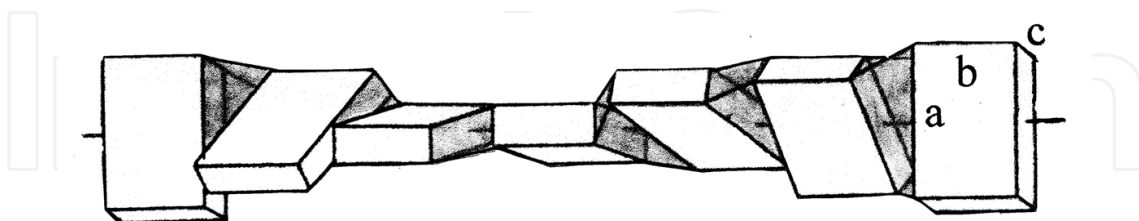


Fig. 9. A schematic structure of the crystal lamella after release of the twist deformation from the ribbon-like lamella. a, b and c (chain axis) correspond to the three cell axes of the orthorhombic crystal and the dark parts represent the inter-grain aggregates. The cell lengths of a, b and c axes for PE are 0.74 nm, 0.49 nm and 0.25 nm, respectively.

Table 5 shows the values of T_c ($\approx T_g^*$), T_b^* , Q , ΔH ($=H_m^a - H_c^a$), Δh , h_g^* and h_x for the samples annealed at $T_a = 376.6$ K, 416.6 K and 426.6 K for 1 hour, where T_g^* is the secondary T_g and T_a is the annealing temperature. h_x was found to decrease with an increasing T_a . The values of h_x for "T_a = 416.6 K and 426.6 K"-samples were near $h_x = 2.3$ kJ/mol for the glass with $T_g =$

135 K in Table 2. In the amorphous region of these samples, the ordered parts with the coarse 4/1 helix structure might be formed⁵⁾. The ordered parts in the inter-grain aggregates, being like the crystals of fold-type with h_x^i instead of h_x , could also have the holes as the pair (see Eq. (28)).

Sample T_a/K	T_c K	T_b^* K	Q kJ/mol	ΔH kJ/mol	Δh kJ/mol	h_g^* kJ/mol	h_x kJ/mol
376.6	391.5	392.4	1.79	0.83	-0.96	3.99	3.03
416.6	391.5	392.5	2.38	0.83	-1.55	3.99	2.44
426.6	391.5	393.3	2.85	0.83	-2.02	3.99	1.97

Table 5. The values of T_c ($\approx T_g^*$), T_b^* , Q , ΔH , Δh , h_g^* and h_x for PE films annealed at 376.6 K, 416.6 K and 426.6 K for 1 hour.

5.3 “Crystal / anti-crystal hole” pairs from secondary glass

The crystal length, ζ , as a function of the melting temperature, T_m , is according to Gibbs-Thomson given by:

$$\zeta = \{T_m^\infty / (T_m^\infty - T_m)\} \{2\sigma_e / (\mu h_u)\} \quad (20)$$

where σ_e is the end-surface free energy per unit area for crystals, μ is the conversion coefficient. For PE, $\mu = (10^6/14)$ mol/m³, $h_u = 4.11$ kJ/mol³⁶⁾ and $T_m^\infty = 415$ K^{18, 36)}. σ_e is given as^{25, 43)}:

$$\sigma_e = \mu h_u c^* \{ [RT_m^2 + (H_x - h_x)(T_m^\infty - T_m)] / \{2(H_x - h_x)T_m^\infty\} \} \quad (21)$$

with $H_x = 2h_u - Q_{mv}$, where c^* is the cell length of c-axis. The term of the square bracket in Eq. (21) is dimensionless. Table 6 shows the values of σ_e for “ $T_a = 376.6$ K, 416.6 K and 426.6 K”-samples, together with the values of T_p , T_e^* , h_x , Q_{mv} , ΔQ_m ($= Q_m - h_c$) and ΔQ ($= Q - Q_m$) used in the calculation of σ_e , where T_p is the melting peak temperature and ΔQ is the heat per molar structural unit corresponding to the area of the lower temperature side peak in Fig. 8, contributing to the activation heat required to release the secondary glass state. ΔQ_m is given by:

$$\Delta Q_m = \int_{T_b^*}^{T_e^*} (dQ/dt)(1/\alpha_s) dT \quad (22)$$

where α_s ($= dT/dt$) is the heating rate. T_e^* was derived from Eq. (22) using ΔQ_m in Table 6. The fact that T_e^* was almost equal to that by observation, as shown in Table 6, supported that h_c was due only to the formation of the crystal lamella, thus giving rise to the melting peak on the higher temperature side. T_e^* is also the end temperature of melting for ordered parts of fold-type in the inter-grain aggregates. Upon heating over T_e^* , the flow parts in the amorphous regions should start to participate directly in the melting of crystals. With an increasing T_a , σ_e and h_x decreased, whereas Q_{mv} , ΔQ_m and ΔQ increased. ΔQ should influence h_x . For all samples, the value of σ_e at T_p was 1.3 times larger than that at T_m^∞ ($Q_m = 0$). The experimental values of σ_e from Eq. (20), 30 ~ 90 mJ/m², differed significantly from those in Table 6, probably due to the length of the lamellae after annealing and the use of cooling as the substitute of ζ at T_m ^{23, 44)}.

Sample T_a/K	T_p K	T_e^* K	h_x kJ/mol	Q_m kJ/mol	ΔQ_m kJ/mol	ΔQ kJ/mol	σ_e at T_p mJ/m ²
376.6	401.2	399.2 (397.7)	3.03	1.37	0.48	0.42	16.3 (12.4)
416.6	401.8	400.1 (399.0)	2.44	1.42	0.53	0.96	14.3 (11.1)
426.6	401.9	400.7 (389.7)	1.97	1.52	0.63	1.33	12.9 (10.1)

The values in the parentheses of T_e^* and σ_e columns are the apparent T_e^* by observation and σ_e at $T_m^\infty = 415$ K ($Q_m = 0$), respectively. T_p is corrected by 0.1 K to the lower temperature side.

Table 6. The values of T_p , T_e^* , h_x , Q_m , ΔQ_m , ΔQ and σ_e for PE films annealed at 376.6 K, 416.6 K and 426.6 K for 1 hour.

On the other hand, according to Flory's theory⁴⁵⁾ on the melting of the fringe-type crystals with a finite ζ , σ_e at λ and $(df_u/d\zeta)_\lambda = 0$ is given by:

$$\sigma_e = \mu(RT\zeta/2)[1/(x - \zeta + 1) + (1/\zeta)\ln\{(x - \zeta + 1)/x\}] \quad (23)$$

where λ is the amorphous fraction, f_u is the free energy per molar structural unit for the crystals and x is the degree of polymerization. In this context:

$$2\sigma_e/\zeta = \mu(f_x - f_u) \quad (24)$$

$$f_x' = RT[(1/\zeta)\ln\{(x - \zeta + 1)/x\} - \ln P_c] \quad (25)$$

where P_c , given by $\{(x - \zeta + 1)/x\}^{1/\zeta}$ for fringe-type crystals, is the probability that a sequence occupies the lattice sites of a crystalline sequence. Moreover:

$$f_u - (f_x - f_x') = 0 \quad (26)$$

Eq. (23) is obtained when $\ln P_c = -1/(x - \zeta + 1)$. From Eq. (26), the relations are derived based on f_u and f_x at $f_x' \geq 0$ and those can be grouped into four equilibrium classes (A ~ D) and one non-equilibrium class (X) as shown in Table 7. Class A of $f_x = f_u$ at $f_x' = 0$ shows the dynamic equilibrium relation between the ordered parts and the crystal parts of equivalent fringe-types, leading to $\sigma_e = 0$ in Eq. (24) as expected for highly oriented fibers. For class B, $f_u = -f_x'$ from Eq. (26) with $f_x = 0$ refers to the anti-crystal holes and $f_x = 0$ is assigned to the ordered parts of $\zeta = \infty$. For class C, $f_x = f_x'$ from Eq. (26) with $f_u = 0$ is assigned to the ordered parts of $\zeta \neq \infty$ (i.e., a kebab structure) and $f_u = 0$ to the crystals of $\zeta = \infty$ (i.e., a shish structure). Class D of $f_u (= f_x') = f_x/2$ is related to the equilibrium in crystal and ordered parts. For those with folded chains, the reversible change from crystal or ordered parts to other parts is expected to take place automatically. The relations in class X do not satisfy Eq. (26), suggesting that the holes of class B can not be replaced by the crystals with $\zeta \neq \infty$.

When $f_u = -f_x'$ for class B, the temperature at which the anti-crystal holes disappear (melt), i.e., T_m^h , is given by:

$$T_m^h = T_m^\infty \{1 + 2\sigma_e/(\mu\zeta h_u)\} \quad (27)$$

where h_u , σ_e and ζ are imaged for the anti-crystal holes, and that, the photonic crystals made up only of photons without the mass. According to Eq. (27), T_m^h approaches T_m^∞ with an increasing ζ . However, the interface between the anti-crystal holes and the ordered parts, which satisfy $f_x = 0$ (described below), should work as the reflector of photons attached to the anti-crystal holes. In this case, the even interface made of the folded chain segments should be avoided through the random reflection. At such an interface, from Eq. (24), the following relation of energy balance is derived:

$$h_x - h_u = T_m^h(s_u - s_x) = \sigma_e / (\mu\zeta) \tag{28}$$

where s_u is the entropy per molar unit for the anti-crystal holes. As well as h_u , one mole of units (photons) corresponds to three moles of the oscillators, since three oscillators can be coordinated to each point of the crystal lattice. According to Eq. (28) or (24), the respective interface energies of the hole and the ordered part are compensated each other at the common interface, leading to $f_x = 0$ of class B and further, T_m^h approaches 0 K with an increasing ζ . From the interface at $\zeta = \infty$, the photons are not reflected, and that, do not exist in the holes. This is exactly the real "dark hole". Therefore when the anti-crystal hole of $\zeta = \infty$ is pairing with the neighboring crystal as shown in Fig. 11C, the crystal is set at 0 K. As opposed to Eq. (27), from $f_u = f_x'$ of class D, the T_m of the crystals is derived:

$$T_m = T_m^\infty \{1 - 2\sigma_e / (\mu\zeta h_u)\} \tag{29}$$

Eq. (29) is the same as Eq. (20). In Eq. (29), T_m is T_m^∞ at $\zeta = \infty$ and from Eqs. (27) and (29), $T_m^\infty = (T_m^h + T_m) / 2$ is derived. According to the pair relation, the emission of heat from the anti-crystal holes after crystallization is necessarily linked to the supply of heat of the same quantity to the newly crystallized parts. However T_m^h should be depressed down to T_m by the emission of heat to the outside. For a model of the inter-grain aggregates shown in Fig. 9, the interaction in the inter-grain aggregates and the a - c face of the crystals must be neglected and the ordered parts in the inter-grain aggregates must satisfy Eqs. (1) and (2) at T_g^* . It is thus presumed that over T_g^* , the chains that cross the glass regions give rise to the newly crystallized parts of fringe-type, whereas the folded chain segments around the glass excluded from the ordered parts give rise to the two end-surfaces of the anti-crystal hole with the same ζ as the new crystal. The T_m of the crystals from the secondary glass, being equal to T_m^h , was found to change from T_b^* to T_e^* as a function of ζ in Eq. (29). The time spent from T_b^* to T_e^* was 0.73 s, in which the probability of observing a spontaneous generation of crystallization or melting should be 1/2, according to the uncertainty principle.

f_x'	f_x	f_u	Class
$f_x' = 0$	$f_x = f_u$	$f_u = f_x$	A
$f_x' > 0$	$f_x = 0$	$f_u = -f_x'$	B
	$f_x = f_x'$	$f_u = 0$	C
	$f_x = 2f_u$	$f_u = f_x / 2 = f_x'$	D
$f_x' > 0$	$f_x = 0$	$f_u = f_x'$	X

Table 7. Relations of equilibrium (A ~ D) and non-equilibrium (X) in f_x and f_u at $f_x' \geq 0$ for crystalline polymers⁴⁶.

Fig. 10 shows the schematic behaviors of sequences and photons on the way of crystallization and melting. The heat of emission, ΔU_h , corresponds to ΔQ_m of the area between the observed melting curve (thin line) and the lower temperature side peak curve from T_b^* to T_e^* and the heat of absorption, $\Delta U_m (= \Delta U_h)$, corresponds to ΔQ_m of the under area of the higher temperature side peak curve from T_b^* to T_e^* in Fig. 8. Fig. 11 shows the cross sections of the glass (A) and the “crystal / anti-crystal hole” pair (C). The two end-surfaces of the anti-crystal hole in Fig. 11C contact in equilibrium those of the ordered parts. Supposing that this model of aggregates was valid for the “ $T_a = 416.6$ K”-sample shown in Fig. 8, a derivation of $f_x' (= -f_u) = 0.13$ kJ/mol was obtained from Eq. (24) using the values of σ_e (see Table 6) and $\zeta (= 3.1$ nm) at $T_p = 401.8$ K (see Table 9). Here, f_x is rewritten as f_x^i for the ordered parts in the inter-grain aggregates. Furthermore, under the assumption that the strain energy in the glass should be spent to build the interface between the anti-crystal hole and the ordered part, by substituting $h_c - \Delta H (= 0.06$ kJ/mol) for $h_x^i - h_u$, it was possible to derive $s_u - s_x^i = 0.15$ J/(K mol) at $T_c (= 391.5$ K), where h_x^i and s_x^i are the enthalpy and entropy per molar structural unit for the ordered parts in the inter-grain aggregates. The relation of $h_x^i - h_u \approx h_c - \Delta H (= 0.06$ kJ/mol) could be supported by determining $\sigma_e/(\mu\zeta) = 0.06 \sim 0.07$ kJ/mol in Eq. (28), which was obtained for all samples using ζ and σ_e at T_p . From $f_x^i = 0$, $h_x^i = 4.17$ kJ/mol and $s_x^i = 10.7$ J/(K mol) at T_c were obtained. Moreover, using $h_u = 4.11$ kJ/mol, s_u was 10.9 J/(K mol) at T_c .

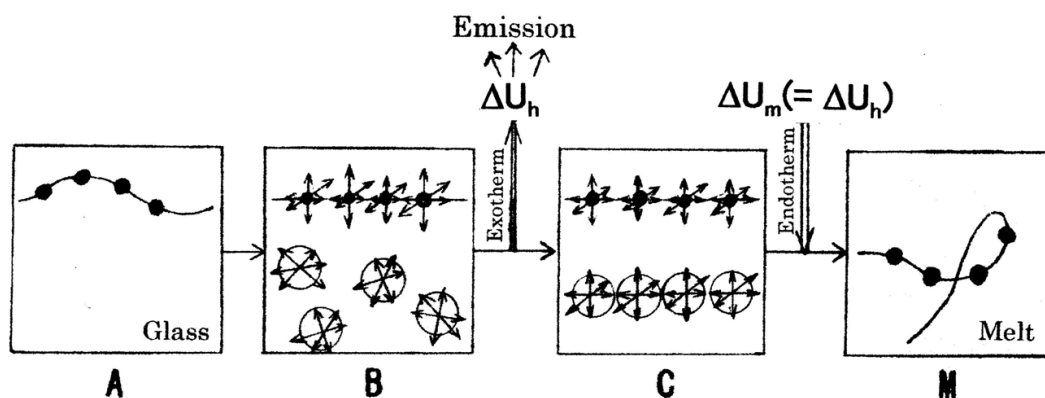


Fig. 10. The schematic process from the glass (A) to the generation of “crystal / anti-crystal hole” pairs (B \rightarrow C) by emission of ΔU_h and then the disappearance of them (M) by absorption of $\Delta U_m (= \Delta U_h)$. The filled circle (\bullet) is the segmental unit, the arrow mark (\leftrightarrow) is the oscillator and the large circle is the photon.

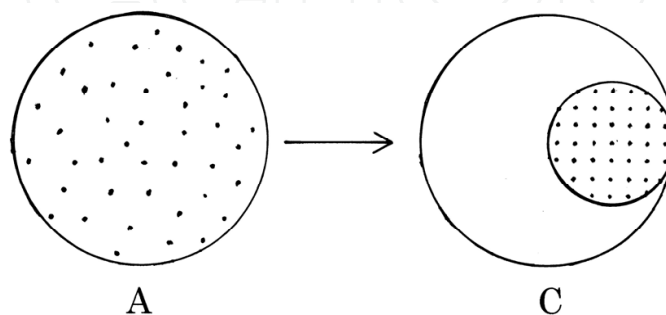


Fig. 11. The cross sections of the glass (A) and the “crystal / anti-crystal hole” pair (C). The dot in large and small circles is the cross section of a segment and the blank in C is the hole. The arrow mark shows the crystallization from A to C.

5.4 Fraction of secondary glass

The anti-crystal holes should be permeated by the photons obeying the frequency distribution function with an upper limit. This is due to the interface between the anti-crystal hole and the ordered part be able to act as a filter for the photons. The molar photon energy loss of the anti-crystal holes, ΔU_h , due to the cavity radiation from T_b^* to T_e^* is given by¹⁸⁾:

$$\Delta U_h = 3C_v^{ph}(T_e^* - T_b^*) \quad (30)$$

On the other hand, the heat change per molar structural unit, ΔU_m , due to the melting of the newly crystallized parts from T_b^* to T_e^* is given by:

$$\Delta U_m = \Gamma \Delta Q_m \quad (31)$$

where Γ is the fraction of the secondary glass, contributed to the generation of "crystal / anti-crystal hole" pairs, in the inter-grain aggregates at temperatures below T_g^* . From $\Delta U_h = \Delta U_m$ at T_e^* , Γ is given by¹⁸⁾:

$$\Gamma = 3C_v^{ph}(T_e^* - T_b^*) / \Delta Q_m \quad (32)$$

Table 8 shows the values of $T_e^* - T_b^*$, Q_m , ΔQ_m , $\Delta U_h (= \Delta U_m)$, $\Delta Q_m / Q_m$ and $\Gamma (= \Delta U_h / \Delta Q_m)$ for PE films annealed at 376.6 K, 416.6 K and 426.6 K for 1 hour. From $\Delta Q_m / Q_m$ and Γ , 35 ~ 41 % of the lamella was constituted of the inter-grain aggregates and approximately 79 ~ 96 % of this was the glass at $T \leq T_g^*$. The difference in ΔQ_m and ΔU_m was believed to represent the irreversible heat change due to the melting of the ordered parts of fold-type, since the folded segments have the excess defect energy. The values of ΔU_h were almost same as $\Delta h (= 0.5 \text{ kJ/mol})$ for the glasses with $T_g = 135 \text{ K}$ and 237 K in Table 2, giving the latent heat required to disappear the holes.

Sample T_a / K	$T_e^* - T_b^*$ K	Q_m kJ/mol	ΔQ_m kJ/mol	ΔU_h kJ/mol	$\Delta Q_m / Q_m$	Γ
376.6	6.8	1.37	0.48	0.46	0.35	0.95
416.6	7.6	1.42	0.53	0.51	0.37	0.96
426.6	7.4	1.52	0.63	0.50	0.41	0.79

Table 8. The values of $T_e^* - T_b^* \rightarrow T_e^* - T_b^*$, Q_m , ΔQ_m , $\Delta U_h (= \Delta U_m)$, $\Delta Q_m / Q_m$ and $\Gamma (= \Delta U_h / \Delta Q_m)$ for PE films annealed at 376.6 K, 416.6 K and 426.6 K for 1 hour.

5.5 ζ distribution function, $F(\zeta)$

The occurrence of ζ distribution by crystallization is one of the characteristics of bulk polymers. The conversion of a DSC melting peak into the ζ distribution by Eq. (20) needs the values of σ_e and T_m^∞ . The σ_e can be evaluated by Eq. (21) using only the DSC data. On T_m^∞ , the inherent temperature of the crystal form should be selected. The $F(\zeta)$ is defined as²⁵⁾:

$$F(\zeta) = (\delta Q_m / Q_m) / \zeta = n_\zeta / \{N_c(T_e - T_b)\} \quad (33)$$

where $\delta Q_m (= \zeta n_\zeta Q_m / \{N_c(T_e - T_b)\})$ is the heat change per molar structural unit per K, n_ζ is the number of crystal sequences with ζ and N_c is the number of structural units of crystals melted in the temperature range from $T_b (= T_b^*$ here) to T_e . $\delta Q_m/Q_m$ is given by:

$$\delta Q_m/Q_m = (dQ/dt) / \int_{T_b}^{T_e} (dQ/dt) dT \quad (34)$$

where dQ/dt is the heat flow rate of the melting curve. Fig. 12 shows $F(\zeta)$ of each melting curve from T_b^* for “ $T_a = 376.6$ K, 416.6 K and 426.6 K”-samples. Table 9 lists the values of ζ -range, ζ_c and ζ_p of $F(\zeta)$ curve for each sample, where ζ_c is ζ at T_e^* and ζ_p is ζ at T_p . For “ $T_a = 376.6$ K”-sample, ζ_p was slightly larger than for other samples. The small value of ζ ($< \zeta_c$) was believed to be caused by the crystallization from the secondary glass in the restricted space of inter-grain aggregates. The large ζ value at the maximum for “ $T_a = 416.6$ K and 426.6 K”-samples might be related to the long period change of lamellae at the higher temperature upon heating³⁶). Whereas, the very narrow ζ -range for “ $T_a = 376.6$ K”-sample might be due to the effective annealing.

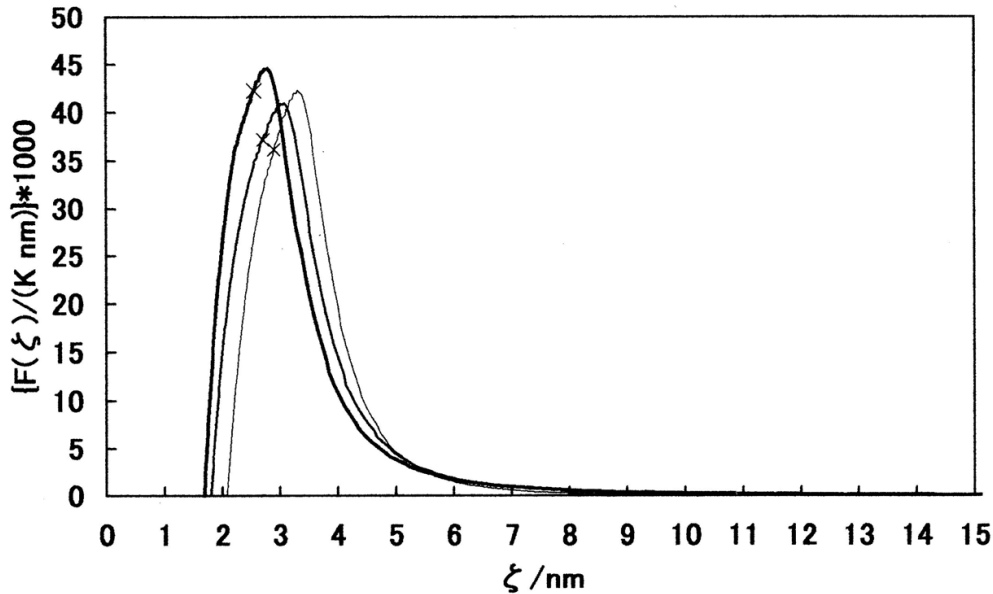


Fig. 12. $F(\zeta)$ for PE films annealed at 376.6 K (right), 416.6 K (middle) and 426.6 K (left) for 1 hour. \times ; $F(\zeta_c)$.

Sample T_a/K	ζ -range nm	ζ_c nm	ζ_p nm
376.6	2.1 - 14	2.9 (2.7)	3.3
416.6	1.8 - 810 ~	2.7 (2.6)	3.1
426.6	1.7 - 730 ~	2.5 (2.2)	2.8

The values in the parentheses are ζ at the apparent T_e^* .

Table 9. The values of ζ -range, ζ_c and ζ_p in $F(\zeta)$ for PE films annealed at 376.6 K, 416.6 K and 426.6 K for 1 hour.

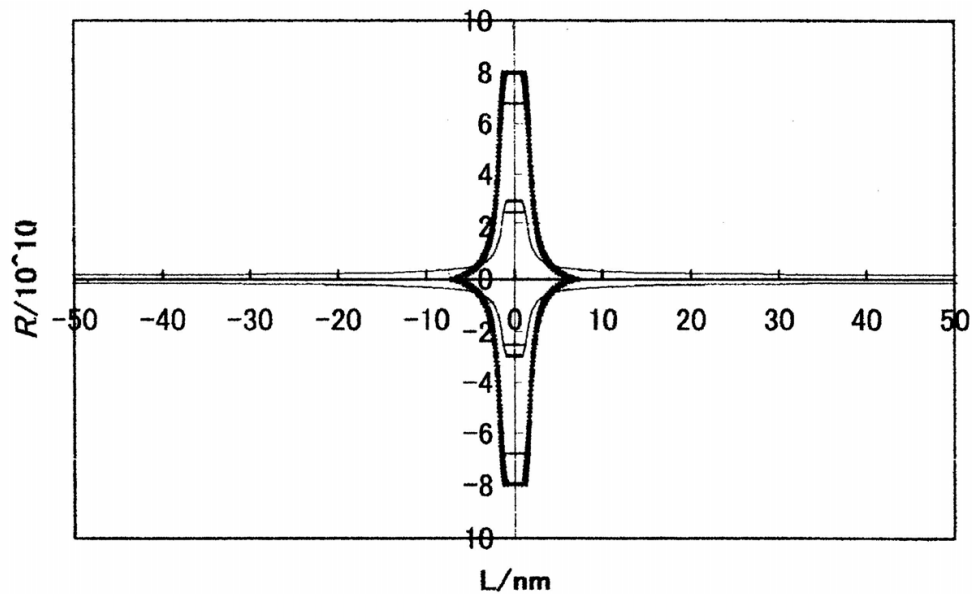


Fig. 13. The relationship between $R (= \pm R_n)$ and $L (= \pm \zeta/2)$ for PE films (1 g) annealed at 376.6 K (thick line) and 426.6 K (thin line) for 1 hour. The horizontal lines show R of the crystal melting from ζ_n or ζ_c to $\zeta = 0$.

In the last stage, a single crystal-like image was drawn from $F(\zeta)$. Rewriting Eq. (33), n_ζ is given by:

$$n_\zeta = F(\zeta)N_c(T_e - T_b) \quad (35)$$

The number of the crystal sequences from ζ_n to ζ , N_ζ , is as follows:

$$N_\zeta = N_c(T_e - T_b) \int_{\zeta_n}^{\zeta} F(\zeta) d\zeta \quad (36)$$

Accordingly, the number of the crystal sequences from $-\zeta (> \zeta)$ to ζ_x , ΔN , is given by:

$$\Delta N = N_c(T_e - T_b) (\int_{\zeta_n}^{\zeta_x} F(\zeta) d\zeta - \int_{\zeta_n}^{\zeta} F(\zeta) d\zeta) \quad (37)$$

where ζ_x and ζ_n are the maximum and minimum of ζ , respectively. When the crystal sequences are bundled, like a fringe in a circle, the number of crystal sequences in a radius direction, R_n , as a function of ζ is given by:

$$R_n = (\Delta N / \pi)^{1/2} \quad (38)$$

Fig. 13 shows the relationship between R ($= \pm R_n$) and L ($= \pm \zeta / 2$) for the samples (1 g) annealed at 376.6 K and 426.6 K for 1 hour. In the ζ -range of $0 \sim \pm \zeta_n / 2$, R at $\zeta_n / 2$ is represented by a solid line, which leads to the supposition of a melting process from the end-surfaces of the crystal with ζ_n at T_b^* . The horizontal line of R at $\zeta_c / 2$ depicts the same imaginable melting process of the crystal with ζ_c at T_e^* . The distinct difference of R or L between both types of crystals should be available in order to evaluate the annealing effects. The single crystal image from R and L for " $T_a = 376.6$ K"-sample (thick line) was very similar to the electron microscope (EM) image of self-seeded PE crystals³⁶.

6. Conclusions

The generation and disappearance of the "crystal / anti-crystal hole" pairs from the secondary glass in PE crystal lamella were discussed on the DSC curves. Thus the fraction of the secondary glass in the lamella was derived from the molar photon energy loss of the anti-crystal holes upon heating, which agreed with the latent heat of disappearance for the holes at the primary T_g of the first order hole phase transition.

7. Acknowledgements

The author wishes to thank Professor em. B. Wunderlich of the University of Tennessee and Rensseler Polytechnic Institute for the encouragement during this work.

8. References

- [1] C. A. Angell, *Science*, 267, 1924(1995).
- [2] F. H. Stillinger, *Science*, 267, 1935(1995).
- [3] P. G. Debenedetti, F. H. Stillinger, *Nature*, 410, 259(2001).
- [4] J. Mainstone, T. Parnell, *Ig Nobel Prize in Physics*, 2005.
- [5] M. R. Tant and A. J. Hill, Ed: "Structure and Properties of Glassy Polymers", Oxford Univ. Press, Oxford, p37, 53(1998).
- [6] T. Hecksher, A. I. Nielsen, N. B. Olsen, J. C. Dyre, *Nature Physics*, 4, 737(2008).
- [7] S. Wei, I. Gallino, R. Busch, C. A. Angell, *Nature Physics*, 7, 178(2011).
- [8] W. L. Johnson, G. Kaltenboeck, M. D. Demetriou, J. P. Schramm, X. Liu, K. Samwer, C. P. Kim, D. C. Hofmann, *Science*, 332, 828(2011).
- [9] F. Zamponi, *Nature Physics*, 7, 99(2011).
- [10] C. A. Angell, I. S. Klein, *Nature Physics*, 7, 750(2011).
- [11] B. Wunderlich, *J. Appl. Polym. Sci.*, 105, 49(2007).
- [12] N. Tanaka, *Polymer*, 19, 770(1978).
- [13] N. Tanaka, *Polymer*, 33, 623(1992).

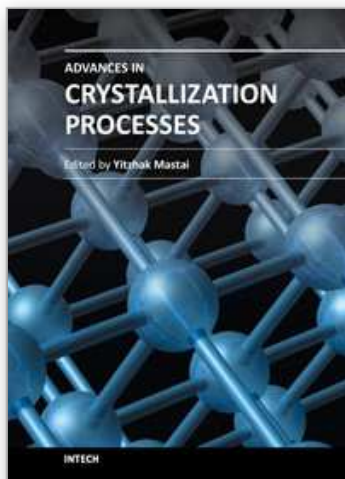
- [14] N. Tanaka, G. Wypych Ed: "Handbook of Solvents", ChemTech Publishing, Tronto, p253(2001).
- [15] N. Tanaka, *Thermochimica Acta*, 374, 1(2001).
- [16] N. Tanaka, Preprints of 46th Japanese Conference on Calorimetry and Thermal Analysis (Tsu), p27(2010).
- [17] ACS, C & EN, October 10, 7(2011).
- [18] N. Tanaka, Preprints of 45th Japanese Conference on Calorimetry and Thermal Analysis (Hachioji), p20(2009).
- [19] L. H. Hill, "Introduction to Statistical Thermodynamics", Addison-Wisley, Massachusetts, p456(1960).
- [20] J. D. Ferry, "Viscoelastic Properties of Polymers", Reinhold, New York, (1961).
- [21] H. Sasabe, K. Sawamura, S. Sawamura, S. Saito, K. Yoda, *Polymer J.*, 2, 518(1971).
- [22] A. Uedono, S. Tanigawa, *Japanese J. Polym.Sci. and Tech.*, 53, 563(1996).
- [23] G. Kanig, *Colloid & Polymer Sci.*, 260, 356(1982).
- [24] T. McLeish, *Physics Today*, 61, No. 8, (2008).
- [25] N. Tanaka, *Polymer*, 49, 5353(2008).
- [26] N. Tanaka, *Polymer*, 34, 4941(1993).
- [27] N. Tanaka, *Polymer*, 35, 5748(1994).
- [28] N. Tanaka, 56th SPSJ Symposium on Macromolecules, *Polymer Preprints (CD)*, Nagoya, 56, (2007).
- [29] B. Wunderlich, ATHAS databank (1992 Recommended Data).
- [30] L. Lew, W. H. de Jeu, "Interfaces and Mesophases in Polymer, Crystallization 2", In: G. Allegra, Ed: *Adv. Polym. Sci.*, 181, Springer, Berlin, p88(2005).
- [31] P. J. Flory, "Statistical Mechanics of Chain Molecules", Wiley & Sons, Inc., New York, (1969).
- [32] Spectroscopical Soc. of Japan, "Infrared and Raman Spectroscopy", Kodansha Sci., Tokyo, (2011).
- [33] J. P. Luongo, *J. Appl. Polym. Sci.*, 3, 302(1960).
- [34] M. Kobayashi, S. Hanafusa, T. Yoshioka, S Koizumi, *Japanese J. Polym.Sci. and Tech.*, 53, 575(1996).
- [35] Y. Yamashita, K. Monobe, *Japanese J. Fiber Sci. and Tech.*, 37, T-53(1981).
- [36] B. Wunderlich, "Thermal Analysis of Polymeric Materials", Springer, Berlin, p141, 247, 659, 780(2005).
- [37] B. Wunderlich, Y. Jin, A. Boller, *Thermochimica Acta*, 237, 277(1994).
- [38] S. Rastigi, A. E. Terry, "Interphases and Mesophases in Polymer, Crystallization 1", In: G. Allegra, Ed: *Adv. Polym. Sci.*, 180, Springer, Berlin, p161(2005).
- [39] Y. K. Kwon, A. Boller, M. Pyda, B. Wunderlich, *Polymer*, 41, 6237(2000).
- [40] J. Pak, B. Wunderlich, *Thermocimica Acta*, 421, 203(2004).
- [41] B. Wunderlich, *Thermochimica Acta*, 446, 128(2006).
- [42] S. Okamura, A. Nakajima, S. Onogi, H. Kawai, Y. Nishijima, T. Higashimura, N. Ise, *Polymer Chemistry*, Kagakudojin, Kyoto, p177(1970).
- [43] N. Tanaka, H. Fujii, *J. Macromol. Sci., Phys.*, B42, 621(2003).
- [44] B. Wunderlich, G. Czornyj, *Macromolecules*, 10, 906(1977).

[45] P. J. Flory, J. Chem. Phys. 17, 223(1949).

[46] N. Tanaka, 58th SPSJ Annual Meeting, Polymer Preprint (CD), Kobe, 58, (2009).

IntechOpen

IntechOpen



Advances in Crystallization Processes

Edited by Dr. Yitzhak Mastai

ISBN 978-953-51-0581-7

Hard cover, 648 pages

Publisher InTech

Published online 27, April, 2012

Published in print edition April, 2012

Crystallization is used at some stage in nearly all process industries as a method of production, purification or recovery of solid materials. In recent years, a number of new applications have also come to rely on crystallization processes such as the crystallization of nano and amorphous materials. The articles for this book have been contributed by the most respected researchers in this area and cover the frontier areas of research and developments in crystallization processes. Divided into five parts this book provides the latest research developments in many aspects of crystallization including: chiral crystallization, crystallization of nanomaterials and the crystallization of amorphous and glassy materials. This book is of interest to both fundamental research and also to practicing scientists and will prove invaluable to all chemical engineers and industrial chemists in the process industries as well as crystallization workers and students in industry and academia.

How to reference

In order to correctly reference this scholarly work, feel free to copy and paste the following:

Nobuyuki Tanaka (2012). Thermodynamics of Enthalpy Relaxation and Hole Formation of Polymer Glasses, *Advances in Crystallization Processes*, Dr. Yitzhak Mastai (Ed.), ISBN: 978-953-51-0581-7, InTech, Available from: <http://www.intechopen.com/books/advances-in-crystallization-processes/thermodynamics-of-enthalpy-relaxation-and-hole-formation-of-polymer-glasses>

INTECH
open science | open minds

InTech Europe

University Campus STeP Ri
Slavka Krautzeka 83/A
51000 Rijeka, Croatia
Phone: +385 (51) 770 447
Fax: +385 (51) 686 166
www.intechopen.com

InTech China

Unit 405, Office Block, Hotel Equatorial Shanghai
No.65, Yan An Road (West), Shanghai, 200040, China
中国上海市延安西路65号上海国际贵都大饭店办公楼405单元
Phone: +86-21-62489820
Fax: +86-21-62489821

© 2012 The Author(s). Licensee IntechOpen. This is an open access article distributed under the terms of the [Creative Commons Attribution 3.0 License](#), which permits unrestricted use, distribution, and reproduction in any medium, provided the original work is properly cited.

IntechOpen

IntechOpen